# Harmonic Structure of Lower Hybrid Waves Driven by Energetic Ions at 4000 km Altitude: PIC Simulation



Geophysical Research Letters

RESEARCH LETTER
10.1029/2022GL102356

**Key Points:**

- The harmonic structure of lower hybrid waves (LHWs) was reported at 4,000 km altitude in the polar region, but its excitation mechanism remains unclear
- We have demonstrated that ring-like energetic ions can generate the harmonic structure of LHWs
- The ion acceleration can be strongly enhanced when the harmonic LHWs can be strongly excited

**Correspondence to:**
T. Kotani,
kotani@kugi.kyoto-u.ac.jp

**Citation:**
Kotani, T., Toida, M., Moritaka, T., & Taguchi, S. (2023). Harmonic structure of lower hybrid waves driven by energetic ions at 4000 km altitude: PIC simulation. *Geophysical Research Letters*, *50*, e2022GL102356. https://doi.org/10.1029/2022GL102356

Received 1 DEC 2022
Accepted 6 FEB 2023



# Harmonic Structure of Lower Hybrid Waves Driven by Energetic Ions at 4000 km Altitude: PIC Simulation

**T. Kotani[1], M. Toida[2,3], T. Moritaka[2,3], and S. Taguchi[1]**

[1]Graduate School of Science, Kyoto University, Kyoto, Japan, [2]National Institute for Fusion Science, Toki, Japan, [3]Department of Fusion Science, SOKENDAI (The Graduate University for Advanced Studies), Toki, Japan

**Abstract** Past satellite observations in the polar region at about 4,000 km altitude have reported lower hybrid waves (LHWs) and their harmonics, but the excitation mechanism of the harmonic LHWs has not yet been clarified. We perform one-dimensional, electromagnetic, full particle-in-cell simulations by setting parameter values in the ranges observed by the satellite. The results from the two runs, that is, for $\omega_{pe}/\Omega_e = 0.1$ and 0.2, show that the energetic ions can generate the harmonic LHWs in both cases. However, in the former case, more harmonic LHWs with larger amplitudes are created and stronger background-ion acceleration is observed. Thus, our present simulations have solved a previously unsolved problem, revealing the possibility that harmonic LHWs are involved in ion acceleration phenomena commonly observed in the polar region, such as ion outflow.

**Plain Language Summary** The lower hybrid waves (LHWs), which can be excited by high-energy ions with an anisotropic velocity distribution, are often observed in the polar region of the Earth's magnetosphere. Recently, increasing attention has been paid to the harmonics of the LHWs, which have been occasionally reported in the Earth's magnetosphere, but their excitation mechanism remains unclear. In this letter, we perform one-dimensional, electromagnetic, particle-in-cell simulations to investigate the development of the LHWs and their harmonic waves. The simulations are based on the observation of harmonic LHWs in the polar region of the Earth's magnetosphere. We have demonstrated that high-energy ions with a ring-like velocity distribution can generate the LHWs and their harmonic waves, and background ions are strongly accelerated when harmonic LHWs are strongly excited. Thus, our simulations have solved a previously unsolved problem, revealing the possibility that the harmonic LHWs are involved in ion acceleration phenomena commonly observed in the polar region, such as ion outflow.

## 1. Introduction

Lower hybrid waves (LHWs) are essentially electrostatic waves often observed in the Earth's magnetosphere. These waves propagate perpendicular to the magnetic field and are characterized by the lower hybrid resonance frequency defined as,

$$\frac{\omega_{LH}^2}{\Omega_i^2} = \frac{1 + (\omega_{pi}/\Omega_i)^2}{1 + (\omega_{pe}/\Omega_e)^2}, \tag{1}$$

where $\omega_{ps} = \sqrt{4\pi n_s q_s^2/m_s}$ is the plasma frequency, $\Omega_s = q_s B/m_s c$ is the cyclotron frequency, and the suffix $s$ denotes particle species ($s = i$ and $e$). In the polar region, the LHWs are believed to play a crucial role in the perpendicular ion heating and subsequent ion outflow (André et al., 1998; Bouhram et al., 2002). The LHWs also play crucial roles in the magnetic reconnection region (Graham et al., 2017). Energetic ions with a ring-like velocity distribution perpendicular to the magnetic field are observed in the polar region (André et al., 1986; Bouhram et al., 2002; Gorney, 1983), and it is now understood that they can excite the LHWs (Akimoto et al., 1985; Cattell & Hudson, 1982).

Past satellite observations at around 4,000 km altitude revealed the presence of the narrowband electrostatic emission at $\omega_{LH}$ (Cattell et al., 2002). Although there are no perpendicularly-propagating waves above $\omega_{LH}$ in the cold plasma approximation, one of these observations has clearly shown the harmonic structure of the LHWs (see Figure 2h in Cattell et al. (2002)). These LHWs and their harmonics are considered to be generated by ring-like energetic ions, but the excitation mechanism of the harmonic LHWs remains unclarified. Furthermore, Huang et al. (2020) reported harmonic LHWs in the magnetotail plasma sheet and suggested that they can be excited by

**Table 1**
*Observed Parameters in the Polar Region by Cattell et al. (2002)*

| | Range |
|---|---|
| Frequency ratio[a] | $0.07 \leq \omega_{pe}/\Omega_e \leq 0.28$ |
| Lower hybrid resonance frequency[a] | $3.15\Omega_i \leq \omega_{LH} \leq 11.6\Omega_i$ |
| Energetic-ion energy | 100 eV to 3 keV |
| Energetic-ion density | 2%–30% |
| Velocity distribution of energetic ions | Ring-like, beam, loss-cone |
| Ion and electron temperatures | Unclear[b] |

[a]The range of $\omega_{pe}/\Omega_e$ can be calculated by $\omega_{pi}^2/\Omega_i^2 = (m_i/m_e)\left(\omega_{pe}^2/\Omega_e^2\right)$ with $m_i/m_e = 1{,}836$ and $10 \leq \omega_{pi}^2/\Omega_i^2 \leq 140$ (paragraph [14] in Cattell et al. (2002)). The range of $\omega_{LH}$ can be calculated by the obtained $\omega_{pe}/\Omega_e$ and Equation 1. [b]Electron temperature at the observed altitudes and latitudes was estimated to be about 5 eV in another study (Kletzing et al., 1998).

non-linear wave-wave coupling. However, the detailed excitation mechanism remains unclear because energetic ions, which are considered to excite the LHWs, were not found in their observation.

Roth and Hudson (1983), Roth and Hudson (1985) performed particle simulations aiming at LHWs with $\omega \lesssim \omega_{LH}$ in the polar region, and their simulations were electrostatic or neglected electron dynamics. So far, no studies have investigated harmonic LHWs in-depth using electromagnetic, full particle-in-cell (PIC) simulations, which are indispensable for investigating the non-linear wave-wave coupling of the harmonic LHWs in low and high frequencies and long and short wavelengths. Hence, this is the first report to investigate the excitation and development of harmonic LHWs driven by energetic ions using one-dimensional, electromagnetic, full PIC simulations based on real observation at 4,000 km altitude in the polar region. We also investigate ion acceleration when harmonic LHWs are excited.

## 2. Simulation Methods and Parameters

In this letter, we perform 1D3V (one-dimensional, three-velocity components), electromagnetic, full PIC simulations, using the code which was used in Moritaka et al. (2016) and now named PASTEL. PIC simulations are commonly used to study ion-ring instabilities that drive the LHWs (Min & Liu, 2015; Toida et al., 2019; Winske & Daughton, 2012, 2015). We use realistic parameters in the simulations based on the observation at 4,000 km altitude (Cattell et al., 2002), as shown in Table 1.

We consider a uniform plasma consisting of background ions, electrons, and energetic ions. The background ions and electrons have Maxwellian velocity distributions at the same temperature, and the energetic ions have an ideal ring-like velocity distribution expressed as follows:

$$f_h(v_\perp, v_\parallel) = \frac{1}{2\pi^{3/2} u_\perp v_{th}} \delta(v_\perp - u_\perp) \exp\left(-\frac{v_\parallel^2}{v_{th}^2}\right), \tag{2}$$

where $v_\perp$ and $v_\parallel$ are energetic-ion velocities perpendicular and parallel to the background magnetic field, respectively, $u_\perp$ is the ring speed, and $v_{th}$ is the thermal velocity of the energetic ions, which is set to be equal to the bulk-ion thermal velocity. Following to previous studies (Roth & Hudson, 1983, 1985), we assume that energetic ions only have a ring-like component. It is a crucial factor in exciting the LHWs, although beam and loss-cone components have been found in the observation (Cattell et al., 2002).

Considering that energetic ions are continuously injected along the magnetic field in the polar region, it is reasonable that we use the energetic-ion injection model in the simulations where energetic ions and the same number of electrons are continuously injected into the plasma. Some simulation studies (Kotani et al., 2021; Toida et al., 2019) have shown that the energetic-ion injection plays a crucial role in the acceleration of background ions and the development of ion-ring instabilities. The position and gyro-phase of these particles are given at random.

The simulations are performed in the $x$-direction with a periodic boundary condition. The background magnetic field ($\boldsymbol{B_0}$) points to the $z$-direction. We consider waves that propagate perpendicular to $\boldsymbol{B_0}$. The simulation length is $L_x \simeq 1.1c/\Omega_e \times 10^3$, with 4,096 spatial grid points. The total number of computational particles is on the order of $10^8$. The time step is $\Omega_e \Delta t \simeq 0.13$.

The other simulation parameters are as follows. The ion-to-electron mass ratio is $m_i/m_e = 1{,}836$. The ratio of the ring speed of the energetic ions to the light speed $u_\perp/c \simeq 0.0025$ corresponds to energy 3 keV. We assume that the density ratio of energetic ions to background ions is zero at $\Omega_i t = 0$ and 20% at the final time step $\Omega_i t \simeq 48$. For this ratio, we use a value slightly larger than the middle of the range reported in the observation by Cattell et al. (2002) (see Table 1), although the choice of this value is somewhat arbitrary. Thus, the values given to the parameters in the simulation are based on the observation.

**Table 2**
*Parameters for Two Different Simulations*

| Case | $\omega_{pe}/\Omega_e$ | $u_\perp/v_A$ | $\beta_e$[a] | Grid separation[b] | $\omega_{LH}$ |
|---|---|---|---|---|---|
| A | 0.2 | 0.022 | $1.4 \times 10^{-5}$ | $4\lambda_D$ | $8.5\Omega_i$ |
| B | 0.1 | 0.011 | $3.6 \times 10^{-6}$ | $2\lambda_D$ | $4.4\Omega_i$ |

[a]Electron thermal velocity is set to be constant for cases A and B. [b]$\lambda_D$ is the Debye length.

In this letter, two cases are considered: $\omega_{pe}/\Omega_e = 0.2$ (case A) and 0.1 (case B). These values are within the range of the observed parameters in Table 1. The value of $\omega_{pe}/\Omega_e = 0.1$ for case B is within the estimated range of $\omega_{pe}/\Omega_e$ when the harmonic LHWs are observed ($0.1 \leq \omega_{pe}/\Omega_e \leq 0.12$). Case A is discussed for comparison with Case B. Other parameters are listed in Table 2.

## 3. Simulation Results

We show that energetic ions can generate harmonic LHWs for both cases. However, the amplitudes and number of harmonic LHWs are much larger for case B than for case A. Moreover, the ion acceleration is enhanced more strongly for case B.

### 3.1. Harmonic Lower Hybrid Waves

Figure 1 depicts the wavenumber-frequency spectra of electric field fluctuations in cases A (left panels) and B (right panels). For case A ($\omega_{pe}/\Omega_e = 0.2$), the strongest LHWs are excited around the lower hybrid resonance frequency, $\omega_{LH} \simeq 8.5\Omega_i (\equiv \omega_1)$ in the period $0 \leq \Omega_i t \leq 24$. The wavenumber is around $k_1 \simeq 500\Omega_i/v_A$, as consistent with the most unstable wavenumber predicted by the linear theory (Kotani et al., 2021). This wavenumber corresponds to $\lambda_1/\rho_i \simeq 4.6$ where $\lambda_1$ is the wavelength, and $\rho_i$ is the ion gyro radius.

Harmonic LHWs are found to be excited around $(mk_1, n\omega_1)$ ($m = 1, 2, 3$ and $n = 0, 1, 2, 3$). Especially, the harmonics are enhanced on the line of $\omega = (\omega_1/k_1)k_x$ indicated by the dashed line in the left-top panel of Figure 1. For $24 \leq \Omega_i t \leq 48$, the enhanced region around $(k_1, \omega_1)$ extends to the larger wavenumber ($k_x v_A/\Omega_i \geq 800$), as shown in their harmonic waves. Although some harmonics near $n\Omega_i$ are excited on the long-wavelength side, their amplitudes are very small due to the cold ring of the energetic ions given by Equation 2 (Roth & Hudson, 1983).

Next, for case B ($\omega_{pe}/\Omega_e = 0.1$), wave amplitudes are small in the period $0 \leq \Omega_i t \leq 24$. However, many harmonic LHWs can be found in the period $24 \leq \Omega_i t \leq 48$. The number of generated harmonic LHWs for case B in this period is larger than those for case A. The strongest LHWs for case B are excited around $(700\Omega_i/v_A, \omega_{LH}) \equiv$

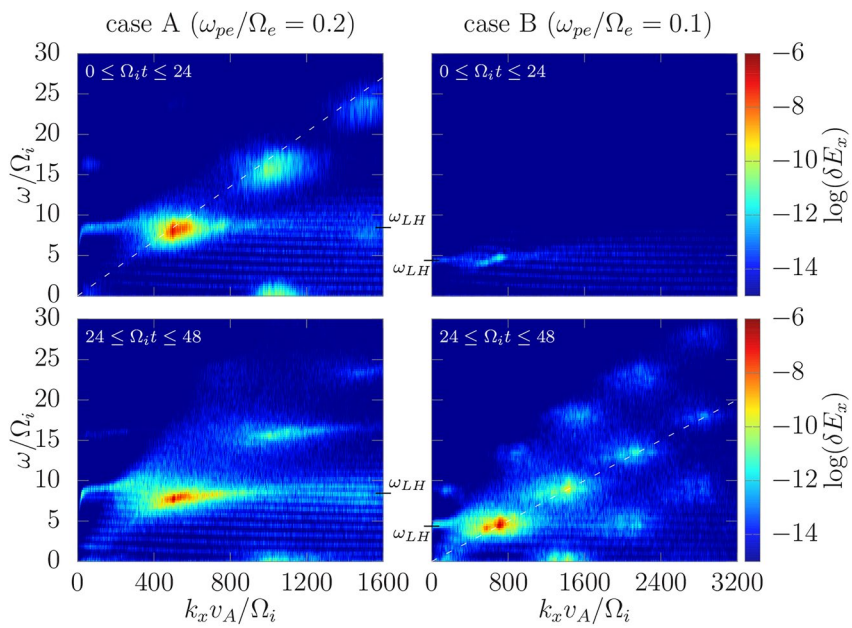


**Figure 1.** Wavenumber-frequency spectra of electric field fluctuations for case A (left panels) and case B (right panels). Two dashed lines indicate the line of $\omega = (\omega_1/k_1)k_x$ (see the main text). Electric and magnetic fields in cgs units are normalized by the background magnetic field unless otherwise noted.

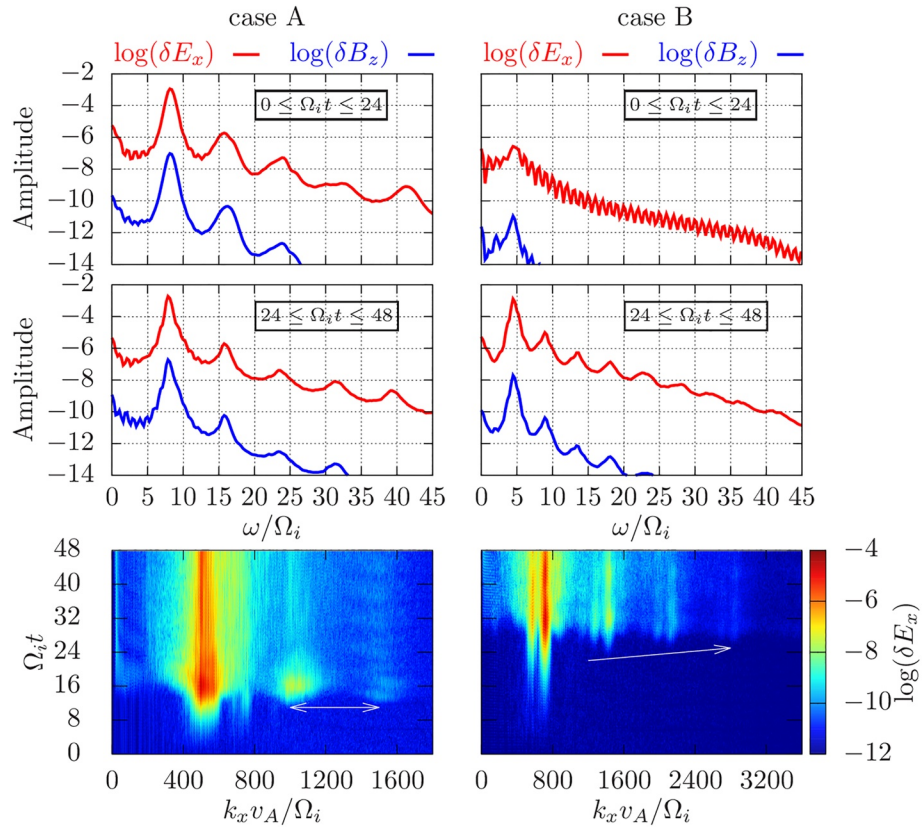


**Figure 2.** (Upper four panels) Frequency spectra of electric (red line) and magnetic (blue line) fluctuations for case A (left panels) and case B (right panels). (Lower two panels) Time wavenumber spectra of electric field fluctuations for case A (left panel) and case B (right panel).

$(k_1, \omega_1)$. The wavenumber corresponds to $\lambda_1/\rho_i \simeq 6.6$. In addition to the waves that appear near the line of $\omega = (\omega_1/k_1)k_x$, many harmonic LHWs are excited below and above this line for case B, which is different from case A.

The harmonic structure of the LHWs is confirmed by frequency spectra of electric and magnetic field fluctuations ($\delta E_x$ and $\delta B_z$) in the upper four panels of Figure 2. This figure is obtained by integrating the Fourier components $\delta E_x(k_x, \omega)$ and $\delta B_z(k_x, \omega)$ over the wavenumber $k_x$. For both cases, the peaks of the harmonic LHWs are seen in $\delta E_x$, while the amplitudes of $\delta B_z$ are much smaller, indicating that the excited waves are almost electrostatic.

However, the two cases differ in the following ways. The amplitudes of the higher harmonics with $\omega \simeq n\omega_{LH} (n \geq 2)$ in case B are much larger than those in case A, although the amplitudes of the fundamentals ($n = 1$) are almost equal for the two cases. If we consider higher harmonics with amplitudes greater than, say, $\log(\delta E_x) = -8$, the number of such harmonics for case B is 4 ($n = 2$, 3, 4, and 5), whereas that for case A is 2 ($n = 2$ and 3). Hence, the number of harmonics for case B is greater than that for case A. Moreover, the difference between amplitudes of $\delta E_x$ and $\delta B_z$ for case B is greater than that for case A, indicating that the excited waves are more electrostatic for case B. Also, the amplitudes of the harmonic LHWs decrease as their order increases. The first peak of $\delta B_z$ is comparable to the third peak of $\delta E_x$ in case A, whereas it is comparable to the fifth peak of $\delta E_x$ in case B.

The lower two panels of Figure 2 depict the time evolution of the wavenumber spectra of electric field fluctuations, $\delta E_x(k_x, t)$. The time development and excitation region of the harmonic LHWs are different between the two cases. In case A, the LHWs begin to grow at $\Omega_i t \simeq 8$ in the broadband wavenumber region, $400 \leq k_x v_A/\Omega_i \leq 600$. The second and third harmonic waves around $k_x v_A/\Omega_i \simeq 1{,}100$ and 1,500 begin to grow at almost the same time, $\Omega_i t \simeq 12$ (see the arrow in the left panel), when the amplitudes of the LHWs exceed $\log(\delta E_x) = -6$. After the amplitudes of the LHWs reach their peak, $\Omega_i t \simeq 17$, the LHWs retain their large amplitudes due to the energetic-ion injection. Conversely, the harmonic LHWs gradually decrease in amplitude.

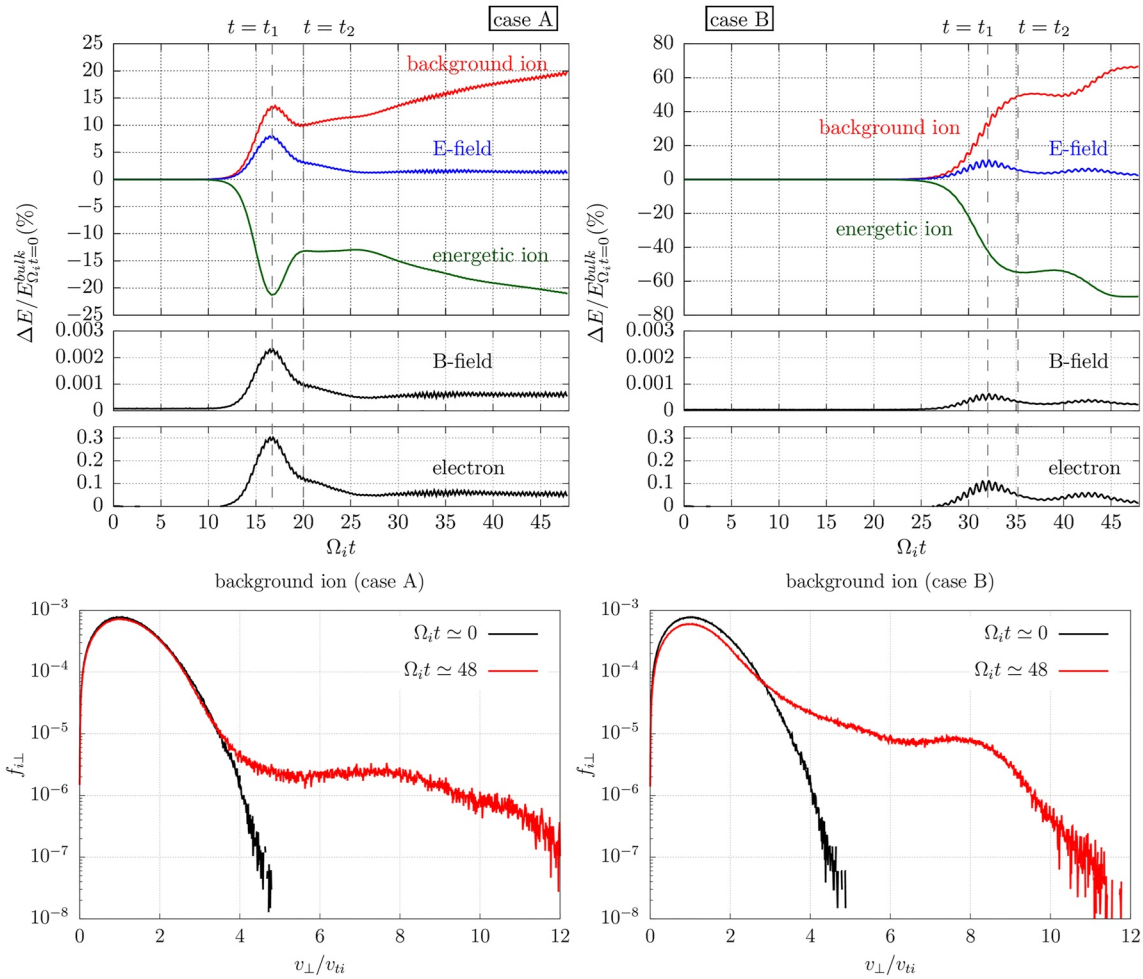


**Figure 3.** (Upper two panels) Energy development of background ions, electric fields (E-field), energetic ions, magnetic fields (B-field), and electrons for case A (left panel) and case B (right panel). Each energy is normalized by the initial energy of background ions. The net energy changes obtained by the difference between the total and injected energies are plotted for energetic ions and electrons. Two dashed lines indicate the times when the electric-field energy reaches the peak ($t = t_1$) and the variation of the energetic-ion energy stops ($t = t_2$). (Lower two panels) Snapshots of the perpendicular velocity distribution of background ions for case A (left panel) and case B (right panel). The horizontal axis is normalized by the bulk-ion thermal velocity.

The LHWs grow more slowly in case B than in case A. Compared to case A, the excitation region of the LHWs and their harmonics are limited in the narrow wavenumber region for case B. When the amplitudes of the LHWs also exceed $\log(\delta E_x) = -6$, the harmonic LHWs begin to grow at $\Omega_i t \simeq 25$. Despite minor differences, the harmonic LHWs grow slower as their wavenumber increases (see the arrow in the right panel). Moreover, the harmonic LHWs around $k_x v_A/\Omega_i \simeq 1{,}500$ retain large amplitudes, unlike in case A. This wavenumber corresponds to the harmonic LHWs with $\omega = 2\omega_{LH}$ and $4\omega_{LH}$, as shown in Figure 1.

Thus, our simulation results have shown that ring-like energetic ions can generate the harmonic LHWs using realistic parameters consistent with those reported by Cattell et al. (2002). We have also found that $\omega_{pe}/\Omega_e$ influences the development of the LHWs and their harmonics.

### 3.2. Energy Development

Figure 3 depicts the energy development of background ions, electric fields, energetic ions, magnetic fields, and electrons in both cases. Because the energy changes of the magnetic field and electrons are significantly small, we focus on the energy development of the bulk ions, electric fields, and energetic ions. Background ions are accelerated by the energetic-ion injection for both cases, but the energy development differs between the two cases. The ratio of injected energy to background-ion energy in case A is the same as in case B.

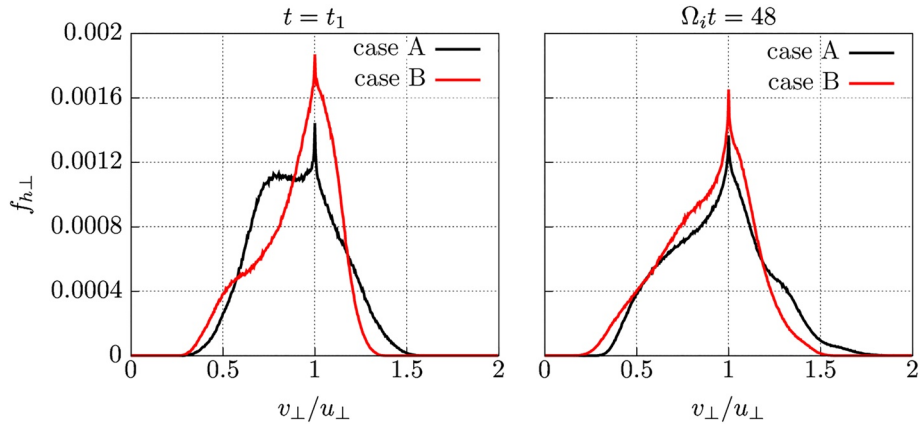


**Figure 4.** Snapshots of the perpendicular velocity distribution of energetic ions for case A and case B at $t = t_1$ (left panel) and $\Omega_i t \simeq 48$ (right panel). The horizontal axes indicate the velocity of the energetic ions normalized by the ring speed.

In case A, the electric-field energy reaches the peak at $\Omega_i t \simeq 17$ ($t = t_1$), consistent with the peak time of the LHW amplitudes. Simultaneously, the background-ion energy reaches the local maximum, whereas the energetic-ion energy reaches the local minimum. At $\Omega_i t \simeq 20$ ($t_2$), the variation of the energetic-ion energy stops, which does not change until $\Omega_i t \simeq 27$. The background-ion energy increases during this period, whereas the electric-field energy decreases. After $\Omega_i t \simeq 27$, the background-ion energy increases, whereas the energetic-ion energy decreases. Finally, at $\Omega_i t \simeq 48$, the background ions are accelerated by 20% of their initial energy. The ion acceleration is also confirmed by the perpendicular velocity distribution of the background ions in the left-bottom panel of Figure 3. The number of background ions for $v_\perp \geq 4v_{ti}$ considerably increases at $\Omega_i t \simeq 48$.

In case B, background ions are accelerated more strongly than in case A. At the final step, $\Omega_i t \simeq 48$, the background ions are accelerated by more than 60% of their initial energy, which is three times of case A. The detailed time development is as follows. Although the background-ion and energetic-ion energies do not reach the local maximum and minimum, the electric-field energy reaches its peak at $\Omega_i t \simeq 32$ ($t_1$), different from case A. At $\Omega_i t \simeq 35$ ($t_2$), the variations of the background-ion and energetic-ion energies stop for the first time. The energy increase of the background ions at this time is already much larger than that at $\Omega_i t \simeq 48$ for case A. After $\Omega_i t \simeq 40$, the background-ion energy increases, whereas the energetic-ion energy decreases again. The energy changes of the magnetic fields and electrons are smaller than those for case A. The strong ion acceleration is confirmed in the background-ion velocity distribution, $f_{i\perp}$. The number of background ions for $4v_{ti} \leq v_\perp \leq 9v_{ti}$ is much larger for case B, although that for $v_\perp \geq 9v_{ti}$ is larger for case A. These results indicate that background ions can be accelerated more strongly for lower $\omega_{pe}/\Omega_e$ where many harmonic LHWs are excited, as shown in Figure 1.

To investigate the difference in energy development between the two cases, we compare the perpendicular velocity distributions of energetic ions in Figure 4. We have found that the difference in the velocity distribution can be responsible for the different energy development. In the linear theory, the ability to excite the LHWs is weaker as the gradient of the perpendicular velocity distribution $\left(\frac{\partial f_{h\perp}}{\partial v_\perp}\right)$ is smaller. However, in the energetic-ion injection model used in the simulations, the injection can sustain large $\frac{\partial f_{h\perp}}{\partial v_\perp}$ even after the collapse of $f_{h\perp}$ (for details, see Kotani et al. (2021)). Figure 4 shows that $\frac{\partial f_{h\perp}}{\partial v_\perp}$ is larger for case B than for case A at both time $t = t_1$ and $\Omega_i t = 48$. This means that the velocity distribution of the energetic ions less violently collapses for case B compared to case A, and the LHWs can be more strongly excited by the injection of energetic ions for case B than for case A. The difference in the non-linear development of $f_{h\perp}$ can explain not only the difference in the energy development but also partially explain the difference in the generation of the harmonic LHWs between the two cases.

## 4. Summary and Discussion

In summary, we have performed one-dimensional, electromagnetic, full PIC simulations to investigate the excitation and development of the harmonic LHWs whose excitation mechanism is unknown. We have demonstrated that ring-like energetic ions can generate the harmonic LHWs at 4,000 km altitude in the polar region using realistic parameters in the ranges consistent with those reported by the observation (Cattell et al., 2002), The

wavenumbers and frequencies of the harmonic LHWs are multiples of those of the LHWs. We have examined the two cases ($\omega_{pe}/\Omega_e = 0.2$ and 0.1) and found that the amplitudes and number of the harmonic LHWs are significantly larger for $\omega_{pe}/\Omega_e = 0.1$. Since $\omega_{pe}/\Omega_e = 0.1$ is consistent with the observation (Cattell et al., 2002), our simulations have solved a previously unsolved problem.

We have also investigated the ion acceleration and found that the background ions are accelerated by the excited waves for both cases. This acceleration is considered to be due to lower hybrid turbulence driven by the excitation in the broadband wavenumber range of the LHWs (Bingham et al., 2002; McBride et al., 1972). The energetic-ion injection can enhance such acceleration (Kotani et al., 2021). Furthermore, we have shown that the background ions are accelerated more strongly for $\omega_{pe}/\Omega_e = 0.1$, where the many harmonic LHWs are strongly excited. This may be explained by the enhanced turbulence due to the strong excitation of the harmonic LHWs. Thus, it has revealed the possibility that the harmonic LHWs are involved in ion acceleration phenomena commonly observed in the polar region, such as ion outflow.

The excitation of the harmonics LHWs may be due to the non-linear wave-wave coupling, not due to the destabilization of the linear-mode waves. In our simulations, the ion Bernstein and ion cyclotron waves due to the energetic ions (Goede et al., 1976) are excited above $\omega_{LH}$, but they cannot explain the harmonics at $n\omega_{LH}$ because these two waves can be destabilized around $\omega \sim n\Omega_i$. In addition to the harmonic LHWs, we have found some interesting results: difference in non-linear development between the two cases and possibility that the harmonic LHWs enhance ion acceleration. In the future, parametric simulations and theoretical analyses will be conducted to investigate our findings in more detail.

Note that lower hybrid solitary structure (LHSS) and broadband ELF (BBELF) waves have been considered as important driving sources for the ion outflow acceleration. In LHSS, electric fields with frequencies around $\omega_{LH}$ and a spatial scale of the order of $\rho_i$ are observed (Schuck et al., 2003). BBELF waves have a broadband frequency spectrum below and around $\Omega_i$ (Knudsen et al., 1998). Considering that the wavenumber range of the excited LHWs is on the order of $\rho_i$ and that one of the harmonic LHWs is excited below $\Omega_i$ (see the region around ($2k_1$, $\omega \lesssim \Omega_i$) in Figure 1), we infer that the LHWs produced in the present simulations are phenomena closely related to LHSS and/or BBELF.

## Data Availability Statement

The simulation data used in this study and scripts to produce the figures are available online https://doi.org/10.5281/zenodo.7375165.

**Acknowledgments**
This work was performed on the "Plasma Simulator" (NEC SX-Aurora TSUBASA) of NIFS with the support and under the auspices of the NIFS Collaboration Research program (NIFS21KNSS164, NIFS22KISS008, and NIFS22KISS016). This work was supported by JST SPRING, Grants JPMJSP2110, JSPS KAKENHI Grants 22J15207, and 22K03570. This work is supported by the "Joint Usage/Research Center for Interdisciplinary Large-scale Information Infrastructures" and the "High Performance Computing Infrastructure" in Japan (Project ID: JH210005-NAH and JH220004-NAH).

## References

Akimoto, K., Papadopoulos, K., & Winske, D. (1985). Lower-hybrid instabilities driven by an ion velocity ring. *Journal of Plasma Physics*, *34*(3), 445–465. https://doi.org/10.1017/S0022377800003007

André, M., Norqvist, P., Andersson, L., Eliasson, L., Eriksson, A. I., Blomberg, L., et al. (1998). Ion energization mechanisms at 1700 km in the auroral region. *Journal of Geophysical Research*, *103*(A3), 4199–4222. https://doi.org/10.1029/97JA00855

André, M., Temerin, M., & Gorney, D. (1986). Resonant generation of ion waves on auroral field lines by positive slopes in ion velocity space. *Journal of Geophysical Research*, *91*(A3), 3145–3151. https://doi.org/10.1029/JA091iA03p03145

Bingham, R., Dawson, J. M., & Shapiro, V. D. (2002). Particle acceleration by lower-hybrid turbulence. *Journal of Plasma Physics*, *68*(3), 161–172. https://doi.org/10.1017/S0022377802001939

Bouhram, M., Dubouloz, N., Malingre, M., Jasperse, J. R., Pottelette, R., Senior, C., et al. (2002). Ion outflow and associated perpendicular heating in the cusp observed by interball auroral probe and fast auroral snapshot. *Journal of Geophysical Research*, *107*(A2), SMP4-1–SMP4-13. https://doi.org/10.1029/2001JA000091

Cattell, C., & Hudson, M. (1982). Flute mode waves near $\omega$ lh excited by ion rings in velocity space. *Geophysical Research Letters*, *9*(10), 1167–1170. https://doi.org/10.1029/GL009i010p01167

Cattell, C., Johnson, L., Bergmann, R., Klumpar, D., Carlson, C., McFadden, J., & Pfaff, R. (2002). Fast observations of discrete electrostatic waves in association with down-going ion beams in the auroral zone. *Journal of Geophysical Research*, *107*(A9), SMP12-1–SMP12-7. https://doi.org/10.1029/2001JA000254

Goede, A., Massmann, P., Hopman, H., & Kistemaker, J. (1976). Ion Bernstein waves excited by an energetic ion beam ion a plasma. *Nuclear Fusion*, *16*(1), 85–96. https://doi.org/10.1088/0029-5515/16/1/009

Gorney, D. J. (1983). An alternative interpretation of ion ring distributions observed by the s3-3 satellite. *Geophysical Research Letters*, *10*(5), 417–420. https://doi.org/10.1029/GL010i005p00417

Graham, D. B., Khotyaintsev, Y. V., Norgren, C., Vaivads, A., André, M., Toledo-Redondo, S., et al. (2017). Lower hybrid waves in the ion diffusion and magnetospheric inflow regions. *Journal of Geophysical Research: Space Physics*, *122*(1), 517–533. https://doi.org/10.1002/2016JA023572

Huang, S. Y., Deng, D., Yuan, Z. G., Jiang, K., Li, J. X., Deng, X. H., et al. (2020). First observations of magnetosonic waves with nonlinear harmonics. *Journal of Geophysical Research: Space Physics*, *125*(6), e2019JA027724. https://doi.org/10.1029/2019ja027724

Kletzing, C. A., Mozer, F. S., & Torbert, R. B. (1998). Electron temperature and density at high latitude. *Journal of Geophysical Research*, *103*(A7), 14837–14845. https://doi.org/10.1029/98JA00962

Knudsen, D. J., Clemmons, J. H., & Wahlund, J.-E. (1998). Correlation between core ion energization, suprathermal electron bursts, and broadband elf plasma waves. *Journal of Geophysical Research*, *103*(A3), 4171–4186. https://doi.org/10.1029/97JA00696

Kotani, T., Toida, M., Moritaka, T., & Taguchi, S. (2021). Pic simulation of energetic-ion injection effects on nonlinear development of lower hybrid wave instabilities. *Journal of the Physical Society of Japan*, *90*(12), 124501. https://doi.org/10.7566/JPSJ.90.124501

McBride, J. B., Ott, E., Boris, J. P., & Orens, J. H. (1972). Theory and simulation of turbulent heating by the modified two-stream instability. *The Physics of Fluids*, *15*(12), 2367–2383. https://doi.org/10.1063/1.1693881

Min, K., & Liu, K. (2015). Fast magnetosonic waves driven by shell velocity distributions. *Journal of Geophysical Research: Space Physics*, *120*(4), 2739–2753. https://doi.org/10.1002/2015JA021041

Moritaka, T., Kuramitsu, Y., Liu, Y.-L., & Chen, S.-H. (2016). Spontaneous focusing of plasma flow in a weak perpendicular magnetic field. *Physics of Plasmas*, *23*(3), 032110. https://doi.org/10.1063/1.4942028

Roth, I., & Hudson, M. K. (1983). Particle simulations of electrostatic emissions near the lower hybrid frequency. *Journal of Geophysical Research*, *88*(A1), 483–488. https://doi.org/10.1029/JA088iA01p00483

Roth, I., & Hudson, M. K. (1985). Lower hybrid heating of ionospheric ions due to ion ring distributions in the cusp. *Journal of Geophysical Research*, *90*(A5), 4191–4203. https://doi.org/10.1029/JA090iA05p04191

Schuck, P., Bonnell, J., & Kintner, P. (2003). A review of lower hybrid solitary structures. *IEEE Transactions on Plasma Science*, *31*(6), 1125–1177. https://doi.org/10.1109/TPS.2003.822043

Toida, M., Igami, H., Saito, K., Akiyama, T., Kamio, S., & Seki, R. (2019). Simulation study of energetic ion driven instabilities near the lower hybrid resonance frequency in a plasma with increasing density. *Plasma and Fusion Research*, *14*, 3401112. https://doi.org/10.1585/pfr.14.3401112

Winske, D., & Daughton, W. (2012). Generation of lower hybrid and whistler waves by an ion velocity ring distribution. *Physics of Plasmas*, *19*(7), 072109. https://doi.org/10.1063/1.4736983

Winske, D., & Daughton, W. (2015). Influence of plasma beta on the generation of lower hybrid and whistler waves by an ion velocity ring distribution. *Physics of Plasmas*, *22*(2), 022102. https://doi.org/10.1063/1.4906889